Inorganic Chemistry

Article

pubs.acs.org/IC

Solvation-Induced Helicity Inversion of Pseudotetrahedral Chiral Copper(II) Complexes

Anne-Christine Chamayou,[†] Gamall Makhloufi,[‡] Laurence A. Nafie,[§] Christoph Janiak,[‡] and Steffen Lüdeke*,[†]

[†]Institut für Pharmazeutische Wissenschaften, Universität Freiburg, Albertstr. 25, D-79104 Freiburg, Germany

[‡]Institut für Anorganische Chemie und Strukturchemie, Universität Düsseldorf, Universitätsstr. 1, D-40225 Düsseldorf, Germany

[§]Department of Chemistry, Syracuse University, Syracuse, New York 13244-4100, United States

Supporting Information

ABSTRACT: The helicity of four-coordinated nonplanar complexes is strongly correlated to the chirality of the ligand. However, the stereochemical induction of either the Δ- or the Λ-configuration at the metal ion is also modulated by environmental factors that change the conformational distribution of ligand rotamers. Calculation of the potential energy surface of bis{(*R*)-*N*-(1-(4-X-phenyl)ethyl)salicylaldiminato-κ^2N,O}copper(II) with X = Cl at the density functional theory level showed a clear dependence of the helicity-determining angle θ between the two coordination planes on the relative population of different ligand conformers. The influence of different substituents (X = H, Cl, Br, and OCH_3) on complex helicity was studied by determination of the absolute configuration at the metal ion in complexes with either (*R*)- or (*S*)-configured ligands. X-ray single-crystal analysis showed that (*R*)-configured ligands with H, Cl, Br induce Δ, while OCH_3-substituted (*R*)-configured ligands induce Λ in the solid state. According to vibrational circular dichroism and electronic circular dichroism studies in solution, however, all tested complexes with (*R*)-ligands exhibited a propensity for Δ, with high diastereomeric ratio for X = Cl and X = Br and moderate diastereomeric ratio for X = H and X = OCH_3 substituted ligands. Therefore, solvation of copper complexes with X = OCH_3 goes along with helicity inversion. This solid-state versus solution study demonstrates that it is not sufficient to determine the chiral-at-metal configuration of a compound by X-ray crystallography alone, because the solution structure can be different. This is particularly important for the use of chiral-at-metal complexes as catalysts in stereoselective synthesis.

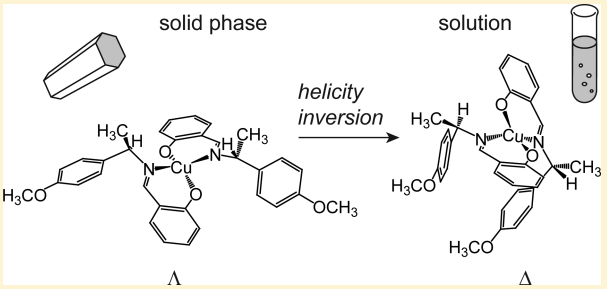

INTRODUCTION

Different from pairs of enantiomers, for diastereomers there exists an energy difference that renders one of them thermodynamically favorable over the other. This energy difference can cause chirality transfer from a primary to a newly formed chiral center. In organic synthesis kinetic effects may play an important role, too.[1] If stable bonds, such as carbon−carbon bonds, are formed, one diastereomer cannot be easily interconverted into the other. However, if weaker interactions are involved in the formation of an additional chiral center, chiral induction depends on thermodynamic equilibria. Examples for thermodynamically driven diastereoselectivity are the formation of suprachiral aggregates, such as fibrillary structures,[2] host−guest systems with guest-specific helicity,[3] and chiral-at-metal complexes,[4] provided that the ligand−metal coordination bonds are weak and labile enough to allow for a thermodynamic equilibrium. In such chiral-at-metal complexes the metal-centered configuration Δ or Λ (Scheme 1)[5] can be induced by the (*R*)- or (*S*)-chirality of the ligand.[4a,6]

Studies on chiral-at-metal complexes, and steric factors that govern the diastereoselectivity on metal-centered chirality formation, had initially been motivated by their important role in asymmetric catalysis; a popular example is the chirality of octahedral complexes of trivalent metals with binaphthalene-derived ligands.[7] The Δ/Λ-configuration can often be determined in a straightforward way. In the solid state, it is easily revealed by X-ray crystallography, making use of resonant (anomalous) scattering of the metal ion.[8] Solutions of chiral-at-metal complexes can be studied by chiroptical methods, such as electronic circular dichroism (ECD),[9] vibrational circular dichroism (VCD),[10] or the measurement of the optical rotation.[11] CD arises from the difference in absorption of left and right circularly polarized light. In chiral-at-metal complexes this is due to a helical disposition of transition dipoles in a chiral molecule.[12] Metal−ligand or metal−metal transitions excited by UV or visible light may result in characteristic signals in the ECD, whose sign is indicative of the metal

Received: November 7, 2014
Published: February 19, 2015

DOI: 10.1021/ic502661u
Inorg. Chem. 2015, 54, 2193−2203

Scheme 1. Enantiomeric Absolute Configurations of a Nonplanar Bis-Chelate Complex Viewed along the C_2 Axis[a]

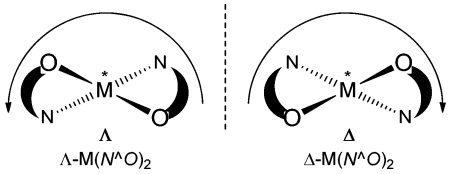

[a] Λ left-handed helicity, Δ right-handed helicity along principal C_2 axis (perpendicular to the paper plane). N and O convey the chelate ring asymmetry.

configuration.[5b,9a,10e,13] In the infrared, coupled vibrations of helically arranged ligand atoms may lead to strong VCD bands that are significantly different or even absent in the free ligand spectrum. This coupled oscillator effect has been used for VCD-based characterization of metal-centered chirality in the past.[10c,d,14]

In chiral catalysts,[15] or bioactive compounds with Δ/Λ-configuration, the metal−ligand coordination is usually strong enough to render the metal inert.[16] However, in complexes with weaker coordination, the configuration at the chiral metal atom may be subject to an equilibrium with the diastereoselective induction depending on the supramolecular interactions with the second coordination sphere that is the surrounding environment. In solution, where an ensemble of different chiral ligand conformers is present, one metal configuration may only exist with some conformers, while others prefer the opposite configuration. The conformer distribution itself may be subject to parameters such as solvent,[10g,17] pH,[18] or the redox state of the metal ion.[19]

Recently, we presented chiral-at-metal tetrahedral zinc complexes that exclusively crystallize with a Λ-configured metal atom in the presence of an (*R*)-configured salicylaldimine-ligand but exhibit a thermodynamic equilibrium between Λ and Δ in solution. This is due to what we would call "chiral cooperative" interactions in a crystal lattice, which are not present in solution.[9b,10d]

The helicity of pseudotetrahedral chiral-at-metal complexes is determined by the relative orientation of the chelate ring planes (Scheme 1), given as the angle θ between the two chelate planes. For virtually tetrahedral salicylaldimine zinc(II) complexes θ is close to 90°.[10d] Complexes of copper(II) are often close to planarity,[9b,20] which suggests an increased propensity for inversion of the Δ/Λ-configuration. This is equivalent with helicity inversion that may depend on modifications that are made to the ligand and/or alteration of the second-sphere coordination (environment).

Asymmetric Schiff-base ligands are frequently used in asymmetric catalysis.[21] Salicylaldiminato ligands, such as those used in previous studies on zinc(II) complexes,[10d,22] allow for easy ligand variation and, hence, are good candidates for studying ligand modification effects on the obtuse helicity in pseudotetrahedral copper(II) complexes. The chiral materials are available by condensation of aldehydes with chiral aromatic amines carrying different substituents in the para position of the phenyl ring.

We determined the absolute metal configuration in the solid state of bis{*N*-(1-(4-X-phenyl)ethyl)salicylaldiminato-κ^2N,O}-copper(II) for X = H, Cl, Br, and OCH_3 by X-ray crystallography. The relative energies of different conformers of Δ or Λ-bis(*R*)-{*N*-(1-(4-Cl-phenyl)ethyl)salicylaldiminato-κ^2N,O}copper(II) with different values of θ were calculated at the density functional theory (DFT) level. We calculated VCD spectra for the presumably most abundant conformers and used them for determination of the absolute configuration of copper(II) complexes with the four different para substituents in the solution state by comparison to experimental VCD spectra. The findings from X-ray crystallography and VCD spectroscopy were confirmed by measuring ECD spectra for all complexes, both in the solid state and in the solution state. The results suggest that the ligand conformation, and therefore the metal configuration, strongly depends on the influence of substituent X in para position of the phenyl ring.

RESULTS AND DISCUSSION

Bidentate enantiopure Schiff-base ligands (*R* or *S*)-*N*-(1-(4-X-phenyl)ethyl)salicylaldiminato-κ^2N,O (**1**) were synthesized as described previously.[10d] The reaction of **1** with $Cu(NO_3)_2\cdot 3H_2O$ and triethylamine in methanol afforded the chiral complexes (Δ or Λ-)bis{*N*-(1-(4-X-phenyl)ethyl)-salicylaldiminato-κ^2N,O}copper(II) (**2**) as dark green crystals (Scheme 2). The molecular structures of (*R*)-**2a−d** and (*S*)-**2a−d** from single-crystal X-ray crystallography are shown in Figure 1.

For crystalline **2a−c** a consistent stereochemical induction is observed: complexation with (*R*)-configured **1a−c** affords a Δ-configured copper ion, while the corresponding (*S*)-configured ligands lead to Λ. Interestingly, unsubstituted (X = H) **2a** crystallizes in a side-chain conformation that is different from the one observed for the halogen-substituted species **2b** and **2c**, which exhibit virtually identical rotamers of the side chain at

Scheme 2. Synthesis and Structure of Chiral Schiff Base Metal Complexes

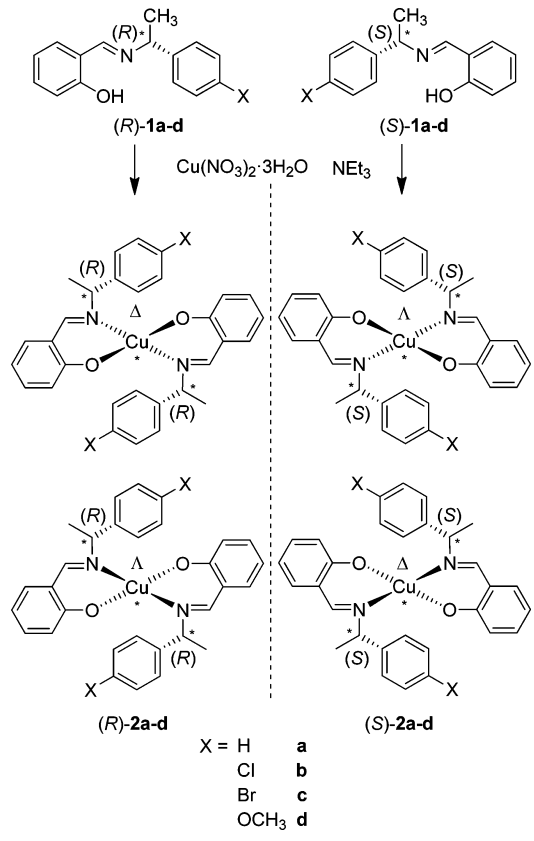

DOI: 10.1021/ic502661u
Inorg. Chem. 2015, 54, 2193−2203

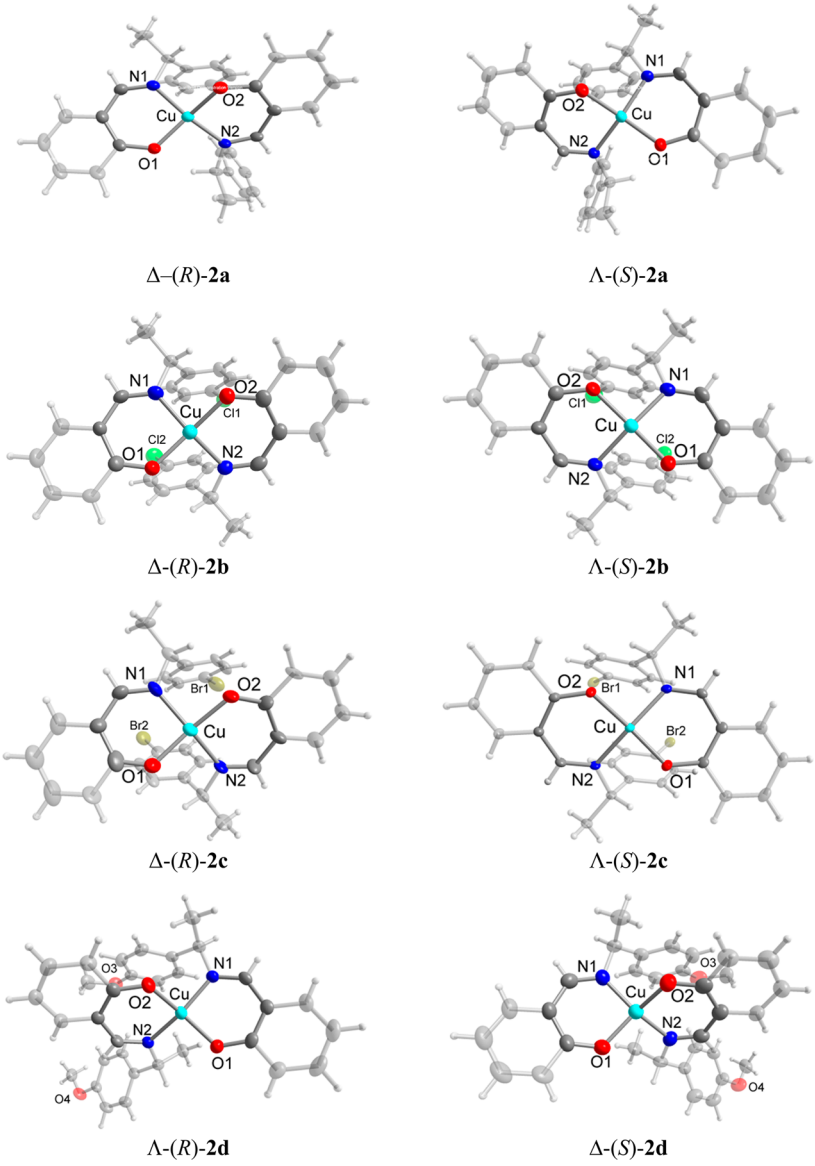

Figure 1. Thermal ellipsoid plots (50% probability) of the enantiomeric copper complexes (*S*)-**2a**–**d** and (*R*)-**2a**–**d** viewed along the pseudo-C_2 axis (perpendicular to the paper plane). The two chelate rings are highlighted. See Figures S1–S8, Supporting Information, for full atom numbering.

N2. Surprisingly, methoxy-substituted **1d** induces the opposite metal-centered chirality in **2d**, namely, Λ-(*R*)-**2d** and Δ-(*S*)-**2d**, respectively. Regarding the data from crystal-structure refinement as based on the absolute structure and Flack parameters between −0.001 and 0.04 (Table S1, Supporting Information)[8] the crystallized materials **2a**–**d** appeared to be enantio- and diastereopure. A Flack parameter close to zero confirms the correct absolute structure and, together with the other refinement parameters, rules out the presence of significant amounts of opposite metal chirality within the investigated crystal. The existence of the other diastereomer being present after formation of a diastereomeric conglomerate cannot be precluded from data based on single-crystal experiments alone. We note, however, that for each complex the corresponding opposite stereochemical induction was observed for all four pairs of enantiomeric ligands, which makes this possibility very improbable.

The different substituents induce a significantly different crystal packing of **2b** and **2c** compared to **2a** and **2d** (see Supporting Information for packing analysis). Both **2b** and **2c** form pseudodimers through a Jahn–Teller elongated Cu···O bond. This results in C_2-related molecules with five-coordinate, square pyramidal copper(II) centers (Figures S9, S11, S13, and S15, Supporting Information). In addition, strong π-stacking interactions involving one of the six-membered, presumably metalloaromatic Cu-chelate rings,[23] may contribute to the pseudodimerization in crystals of **2b** and **2c** (Supporting Information, Figures S10, S12, S14, S16). In contrast, strong intermolecular interactions are missing in **2a** and **2d**. In the case of **2a**, which has a nonfunctional phenylethyl side-chain, the packing is governed by C–H···π interactions. Similarly, for **2d** only intermolecular C–H···O contacts from the methoxy methyl group to the salicyl oxygen atom were found but no intermolecular π–π/C–H···π interactions as in **2b** and **2c**. Therefore, it is not surprising that the different complexes crystallize with different conformations. This in turn seems to induce the configuration at the metal ion: the conformations that are observed for the crystal structures of (*R*)-**2a**, (*R*)-**2b**, and (*R*)-**2c** come along with a Δ-configured copper ion, while

DOI: 10.1021/ic502661u
Inorg. Chem. 2015, 54, 2193–2203

the preferred conformation in the crystal structure of (*R*)-**2d** is compatible with the Λ-configuration.

To study the relationship between the different conformations in complexes **2** and the helicity of the copper coordination we performed a conformational analysis of (*R*)-**2b** as a model for the different salicylaldiminato-copper(II) complexes. The complex structure was separated into two parts. (i) A rigid tetracyclic spiro scaffold with either a Δ or a Λ-configured copper serving as the spiroatom. (ii) Two chiral (4-Cl-phenyl)ethyl side chains attached to N1 and N2 that are freely rotatable around the single bond between either N1 or N2 and the adjacent chiral carbon atom C_α (Figure 2).

We suggest that the rotation around the N−C_α single bonds does not only have an impact on the relative energies, and therefore on the relative population of each conformer, but also determines the metal-centered helicity. A measure for the latter is distortion angle θ, which adopts values between 90° (for tetrahedral complexes) and 0° (for planar complexes). In this context, a change in sign of the value of θ that is triggered by rotation around N−C_α is equivalent to a transition between the Δ and the Λ-configuration. Which sign corresponds to which configuration depends on an arbitrary point of origin. As depicted in Figure 2 plane 1 is defined as the *xy*-plane. We arbitrarily chose a coordinate system that leads to intersection of tilted plane 2 with the *z*-axis at negative values for Δ-configured complexes and therefore to negative values of θ for Δ and positive values of θ for Λ (Table 1).

We calculated potential energy surfaces (PES) with respect to the rotational angles φ_1 and φ_2 around the two N−C_α bonds for Δ-(*R*)-**2b** and Λ-(*R*)-**2b**. To accomplish this, we rotated the (*R*)-(4-Cl-phenyl)ethyl side chains in increments of 20° around either a Δ or the Λ tetracyclic spiro scaffold. As a starting value for θ we chose the value determined from the crystal structure (−34° for Δ and +34° for Λ). These structures were energy minimized for 20 optimization cycles at the B3LYP level using Ahlrichs VTZ[24] for copper and 6-31G(d) for all other atoms as basis sets in GAUSSIAN09.[25] The energy maps and the dependence of θ in respect to the rotational angles after the 20 cycles are shown in Figure 3.

The single point energy (SPE) maps in Figure 3A can be divided into four sections each, which include all the pairs of φ_1 and φ_2 that are sterically possible. However, most pairs of dihedrals are energetically not preferable. Notably, no reasonable energy troughs for particular conformers can be

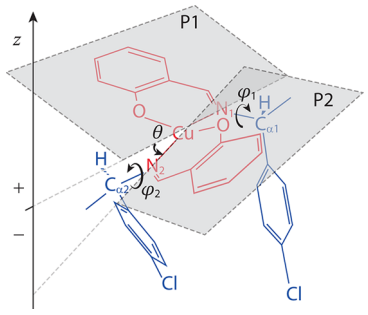

Figure 2. Subunits of Δ-(*R*)-**2b**. Red: rigid tetracyclic spiro scaffold. Blue: (*R*)-(4-Cl-phenyl)ethyl side chains that are rotatable around N_1−$C_{\alpha1}$ (dihedral φ_1) and N_2−$C_{\alpha2}$ (dihedral φ_2). The spiro scaffold spans the two planes P1 and P2 (gray) that are tilted with respect to each other at angle θ, with the plane intersection going through the copper ion (Table 1).

Table 1. Values of θ Calculated from Crystal Structures of (*S*)-2a−d and (*R*)-2a−d

(*R*)-**2a−d**		(*S*)-**2a−d**	
compound	θ^a (deg)	compound	θ^a (deg)
Δ-(*R*)-**2a**	−42.1(1)	Λ-(*S*)-**2a**	+39.07(5)
Δ-(*R*)-**2b**	−34.13(13)	Λ-(*S*)-**2b**	+33.95(7)
Δ-(*R*)-**2c**	−33.26(2)	Λ-(*S*)-**2c**	+32.9(1)
Λ-(*R*)-**2d**	+52.12(5)	Δ-(*S*)-**2d**	−52.48(2)

[a]The sign of θ is arbitrarily chosen to be positive for Λ and negative for Δ.

deduced from the SPE maps at a given θ of ±34°. Both for Δ-(*R*)-**2b** and Λ-(*R*)-**2b** there is no obvious interdependence between φ_1 and φ_2 leading to generation of relative minima on the energy map. This suggests that energy minimization also involves other geometry parameters, such as rotation of the 4-Cl-phenyl-rings and a change in θ. After partial energy minimization the dots representing different starting geometries cluster together at certain positions for φ_1/φ_2 pairs representing relative minima (Figure 3B). These energy troughs were not anticipated from the SPE maps. Their formation coincides with a change in θ (Figure 3C). This suggests that φ_1 and φ_2 induce the angle θ in tetrahedral copper(II) salicylaldiminato complexes, which may depend on steric demand of substituents.

To deduce possible conformers for both Δ-(*R*)-**2b** and Λ-(*R*)-**2b**, we picked representative geometries for each agglomerate of black dots in Figure 3B (13 for Δ-(*R*)-**2b** and 18 for Λ-(*R*)-**2b**), that were probably close to a relative energy minimum. After full geometry optimization and energy minimization at the B3LYP/Ahlrichs VTZ, 6-31G(d) level we removed all duplicates and geometries with negligible Boltzmann populations (calculated with respect to relative energies). Interestingly, one geometry that still had exhibited a Λ-configuration after 20 minimization iterations had converged to a geometry with Δ-configuration after full energy minimization. This suggests that there may be only a small energy difference between some Δ and Λ-conformers with particular values for φ_1 and φ_2 being allowed with a Δ- but not with a Λ-configuration. On the basis of this conformational analysis four Δ-conformers and two Λ-conformers were chosen for geometry optimization and calculation of vibrational frequencies using B3LYP/Ahlrichs VTZ and 6-31G+(d,p) instead of 6-31G(d). The angles θ, φ_1, and φ_2 and the corresponding relative energies for all six conformers after energy minimization at this computational level are listed in Table 2. The Boltzmann distribution for the six conformers suggests no diastereomeric excess (diastereomeric ratio, dr Δ:Λ of 47:53) if calculated with respect to Δ*E* but a clear excess of Δ (dr Δ:Λ of 84:16) if calculated with respect to Δ*G*. A similar dependence on thermochemical contributions had also been observed for chiral tetrahedral complexes of zinc.[10d] Still, the energy difference between the highest populated Δ and the highest populated Λ-conformer is less than 3 kJ·mol^{-1} (Table 2). Although there is an overall propensity for Δ, the lowest energy Λ-conformer has a higher population than the highest energy Δ-conformers. This is consistent with the assumption that different conformations come along with different metal-centered chirality. To validate these results we calculated VCD spectra for the six conformers from Table 2. Comparison of the Boltzmann-averaged spectrum (Figure 4A,II) to an experimental $CDCl_3$ solution spectrum of (*R*)-**2b** (Figure 4A,I)

DOI: 10.1021/ic502661u
Inorg. Chem. 2015, 54, 2193−2203

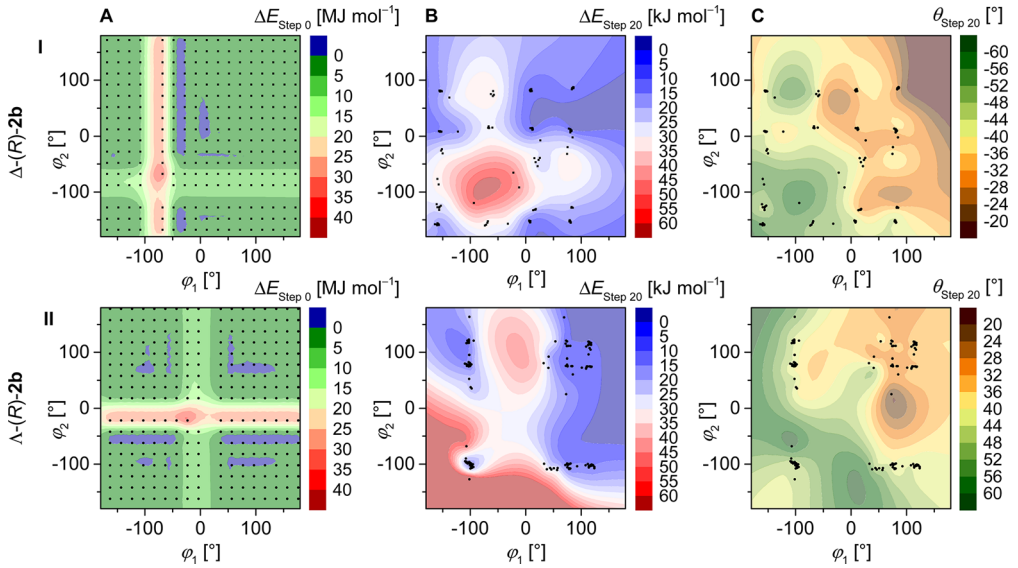

Figure 3. Results from PES scans calculated at the B3LYP/Ahlrichs VTZ, 6-31G(d) level for Δ-(*R*)-**2b** (I) and Λ-(*R*)-**2b** (II). (A) Color coded single point energy maps (relative energies at step 0; no energy minimization) for geometries (black dots) with different dihedrals φ_1 and φ_2 (increments of 20°). Angle θ (−34°) in A, I is taken from the crystal structure of Δ-(*R*)-**2b**. The Λ-geometries in A, II are modeled with the inverted value of θ (+34°). Every dot corresponds to a geometry with one pair of dihedrals. Rows with missing dots correspond to pairs of dihedrals that would generate sterically impossible geometries. (B) Relative energy maps of Δ-(*R*)-**2b** and Λ-(*R*)-**2b** after 20 cycles of energy minimization, already showing a clear trend toward energetically favorable pairs of φ_1 and φ_2. Each black dot represents a relaxed geometry that corresponds to a starting geometry in A clustered around selected φ_1/φ_2 values that are close to a relative minimum. (C) Angle θ (cf. Figure 2) for the relaxed geometries from B. Energy minimization goes along with a change of θ resulting into conformations with more planar and conformations with more pseudotetrahedral geometry.

Table 2. Values of θ, Relative Energies, Relative Free Energies, and Boltzmann-Weights for Different Conformers of Complex (*R*)-2b, Calculated for the Gas Phase at the B3LYP/Ahlrichs VTZ, 6-31+G(d,p) Level

geometry	ΔE (kJ·mol^{-1})	Boltzmann weights (%) in respect to ΔE	ΔG (kJ·mol^{-1})	Boltzmann weights (%) in respect to ΔG	φ_1 (deg)	φ_2 (deg)	θ (deg)
			Δ-(*R*)-**2b**				
conformer 1	2.06	20.8	0	42.0	+16	+15	−35
conformer 2	2.30	18.9	0.11	40.2	+15	+81	−33
conformer 3	5.23	5.8	8.82	1.2	+81	+81	−30
conformer 4	8.71	1.4	12.82	0.2	+13	−153	−43
			Λ-(*R*)-**2b**				
conformer 1	5.77	4.6	7.11	2.4	−102	+79	+41
conformer 2	0	48.1	2.73	13.9	+78	+78	+31

allowed for assignment of the absolute configuration of the excess diastereomer (Δ) and also confirms that the dr is in the range of ∼80:20 as predicted by the model.

The agreement of the calculated and experimental VCD spectra is particularly good for the band pattern at 1630 (+)/1624 (−)/1614 (+) cm^{-1}. These bands correspond to coupled oscillator C═N stretch vibrations with 1630 (+)/1624 (−) indicating Δ- and 1614 (+) indicating Λ-configuration at the metal ion (Figure 4A,III,IV). We compared these bands in the solution VCD spectra of (*R*)-**2a**, (*R*)-**2b**, (*R*)-**2c**, and (*R*)-**2d** (Figure 5).

The very similar spectra and the comparable intensities of coupled oscillator bands at 1630 (+)/1624 (−)/1614 (+) cm^{-1} imply comparable dr for (*R*)-**2b** (chloro) and (*R*)-**2c** (bromo) with excess of the Δ-configuration (Figure 5A,II,III). However, the different relative intensities with a more pronounced positive band at 1614 cm^{-1} indicate considerably lower diastereoselectivity in (*R*)-**2a** (no substituent) (Figure 5A,I) and (*R*)-**2d** (methoxy) (Figure 5A,IV), which suggests a different conformer distribution for (*R*)-**2a** and (*R*)-**2d** compared to (*R*)-**2b** and (*R*)-**2c**. This is in agreement with the observation from X-ray crystallography that **2b** and **2c** crystallize in very similar geometries, while the conformations of **2a** and **2d** are different. For the latter this even leads to the opposite configuration at the copper ion compared to the three other complexes in the solid state (Figure 1). Different from previous studies on salicylaldiminato zinc(II) complexes,[10d,22] the dr determination by ^{1}H NMR experiments is very difficult for paramagnetic copper(II) complexes. On the basis of the assumption that the intensity of the coupled C═N oscillator signals in the VCD can be regarded as virtually independent from the para substituents at the phenyl ring we estimated the dr from the relative band intensities at 1630 (+)/1624 (−)/1614 (+) cm^{-1}. To accomplish this, we calculated the coefficients for constructing the experimental band intensities (Figure 5A,I,IV) by linear combination of the intensities of the corresponding bands (1628, 1621, and 1614 cm^{-1}) calculated for Δ-(*R*)-**2b** and Λ-(*R*)-**2b** (Figure 4A,III,IV). This procedure led to an estimated ratio Δ:Λ ≈ 75:25 for (*R*)-**2b** and for (*R*)-**2c**, which suggests that the theoretically predicted dr of 85:15

DOI: 10.1021/ic502661u
Inorg. Chem. 2015, 54, 2193−2203

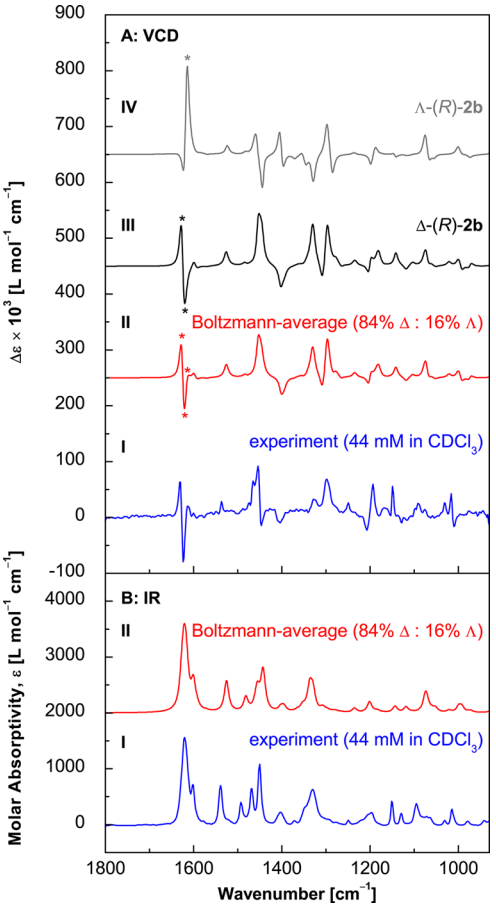

Figure 4. (A) Experimental VCD spectrum, measured for a 2.5% solution of (*R*)-**2b** in $CDCl_3$ (I, blue) compared to spectra calculated for Λ-(*R*)-**2b** (IV, gray), Δ-(*R*)-**2b** (III, black) at the B3LYP/Ahlrichs VTZ, 6-31+G(d,p) level, and a Boltzmann-averaged spectrum (II, red). The band pattern attributed to C═N stretch vibrations used for semiquantitative determination of dr is indicated by asterisks. (B) Experimental (I, blue) and calculated (II, red) IR spectra. Spectra A,II−IV and B,II are offset for better comparison.

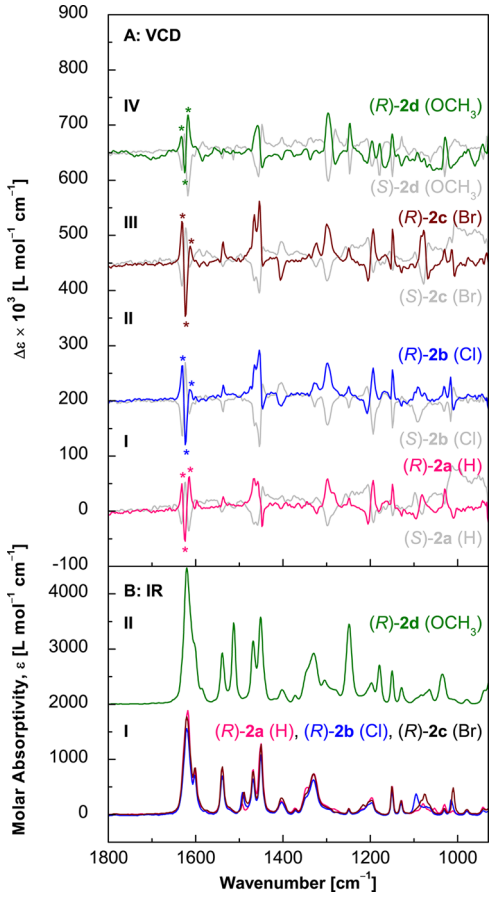

Figure 5. (A) Experimental VCD spectra of (*R*)-**2a** (I, pink), (*R*)-**2b** (II, blue), (*R*)-**2c** (III, brown), and (*R*)-**2d** (IV, green). The corresponding (*S*) enantiomers are shown in gray. The band pattern attributed to C═N stretch vibrations used for semiquantitative determination of dr is indicated by asterisks. The dr is reflected by the relative intensities of the bands. (B) Comparison of superimposed IR spectra of (*R*)-**2a−c** (I) to the IR spectrum of (*R*)-**2d** (II). Spectra A,II−IV and B,II are offset for better comparison.

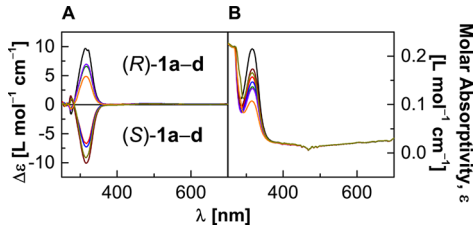

Figure 6. CD (A) and UV−vis absorbance spectra (B) of ligands (*R*)- and (*S*)-**1a−d**.

from calculating the Boltzmann distribution (Table 2) possibly underestimates the contribution of Λ-conformers. The same analysis yields significantly lower dr for (*R*)-**2a** (∼60:40) and (*R*)-**2d** (∼50:50). Because the marker band intensities in the calculated spectra may vary with the respective distribution of Δ- and Λ-conformers, the quantitative value of these numbers is very limited. Nevertheless, it can be stated that the stereochemical induction is considerably weaker for H or OCH_3 in para position than for Cl and Br substituents, thereby leading to only moderate excess of either Δ or Λ in solution.

To confirm the observations from VCD with an additional, independent method that is sensitive toward Δ/Λ-stereoisomerism, we also measured electronic CD (ECD) spectra of all four complexes, both in solution and in the solid state. For this purpose ECD ideally complements VCD. While VCD allows for a very distinct interpretation and assignment of particular bands, which even can be used for a semiquantitative estimation of the conformeric and diastereomeric composition, ECD is very sensitive toward coupled electronic transitions that arise from the helical disposition of electric transition dipoles.[12] A comparison of the ECD spectra of free ligands **1a−d** (Figure 6) shows virtually identical UV-absorbance maxima at 316 nm for all four para substituents, with respective negative CD for all (*R*)-configured ligands and positive CD for all (*S*)-configured ligands. The conserved position of the UV maxima suggests that there is no noticeable auxochromic shift of the electronic transition ($\pi-\pi^*$ of aromatic groups) due to the para substituent.

The ECD of the complexes **2a−d** in chloroform solution shows characteristic bands that are also conserved through all variants (Figure 7A). On the basis of previous assignments from time-dependent (TD) DFT calculations for similar complexes,[9b] we attribute these bands to ligand−metal charge transfer and $\pi-\pi^*$ transitions (270−330 nm), ligand−metal charge transfer (340−415 nm), and metal d−d transitions

DOI: 10.1021/ic502661u
Inorg. Chem. 2015, 54, 2193−2203

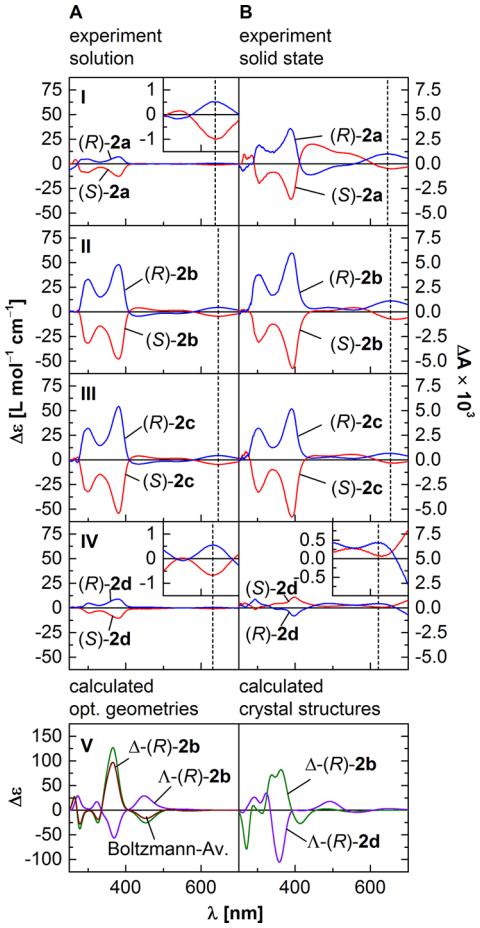

Figure 7. (A) I–IV: Chloroform solution ECD spectra of (*R*)- (blue) and (*S*)-configured (red) **2a–d**. V: Averaged ECD spectra calculated for the conformers of Δ-(*R*)-**2b** (green), Λ-(*R*)-**2b** (purple) on the optimized geometries from the conformational analysis (see above) at the B3LYP/Ahlrichs VTZ, 6-31+G(d,p) level using the Boltzmann-weights from Table 2; the Boltzmann-average over all six conformers is shown in brown. (B) I–IV: ECD spectra of KBr pellets containing 0.1% of complex (blue for (*R*)- and red for (*S*)-**2a–d**); V: ECD spectra calculated on the crystal structure geometries of Δ-(*R*)-**2b** (green), Λ-(*R*)-**2d** (purple). The insets A, I and IV and B, IV show a *y*-expanded detail view between 500 and 700 nm of ECD bands corresponding to d–d transitions. The vertical lines (dashed) indicate the different positions of the corresponding maxima (minima) in each spectrum.

(500–700 nm) in the complex. They all result into bands with opposite sign in the ECD that can be used as an indicator of the metal configuration. This is in particular true for the d–d transition, which generates, albeit with low signal intensity, a characteristic couplet that is due to the asymmetric coordination environment of the copper(II) ion.

In chloroform all bands listed above have the same sign, which suggests that **2a–d** have a conserved configuration at the copper ion in solution. The overall band shape is very similar for **2b**, **2c**, and **2d** but slightly different for **2a**, which exhibits an additional band at ∼268 nm. While the difference in molar absorptivity ($\Delta\varepsilon$) is comparable for **2b** and **2c**, it is significantly lower for **2a** and **2d**. The different para substituents do not lead to different maxima in the ligand spectra and are therefore not likely to have an influence on the transition frequencies in the complex either. However, the substituents might have an impact on the conformer distribution. The different spectral contributions from Δ- and Λ-conformers present with either H, Cl, Br, or OCH_3 in para position may cancel each other and lead to low $\Delta\varepsilon$ for complexes with low dr. Therefore, the low $\Delta\varepsilon$ in the CD spectra of **2a** and **2d** (Figure 7A,I,IV) agrees with the poor dr suggested from the VCD analysis. Different from the semiquantitative VCD-analysis of (*R*)-**2d**, the sign of the low-intensity CD bands in Figure 7A,IV qualitatively indicates a small excess of Δ-configuration in (*R*)-**2d**. However, a quantitative evaluation is not possible without the knowledge of the CD spectrum of diastereomerically pure Δ-(*R*)-**2d** and Λ-(*R*)-**2d** (or Λ-(*S*)-**2d** and Δ-(*S*)-**2d**, respectively). To confirm that spectral contributions from the other diastereomer may lead to cancellation of CD bands we performed TD-DFT calculations on the six conformers of model compound (*R*)-**2b** at the B3LYP/Ahlrichs VTZ, 6-31+G(d,p) level (Figure 7A,V). Both the spectra of Δ-(*R*)-**2b** and Λ-(*R*)-**2b** diastereomer exhibit a strong CD band at 365 nm, which agrees well with the ligand–metal charge transfer bands observed in the experimental spectra. All bands seem to have opposite sign, which confirms the assumption that a low dr may be the reason for the low signal intensity in spectra of **2a** and **2d**.

Summarizing the conclusions that can be drawn from VCD and ECD solution spectra, there seems to be a high degree of induction of metal-centered chirality, namely, Δ-(*R*) or Λ-(*S*) in **2b** and **2c**, while the relative VCD intensities of the band pattern at 1630 (+)/1624 (−)/1614 (+) cm^{-1} (Figure 5A,I,IV) and the low ECD intensities in Figure 7A,I,IV, indicate that chirality transfer is significantly less pronounced in **2a** and **2d**. X-ray crystallography, on the other hand, showed Δ-(*R*) or Λ-(*S*) induction in **2a–c**, but the opposite induction, Δ-(*S*) or Λ-(*R*), in methoxy-substituted **2d**. Therefore, compared to solution spectra, for solid-state ECD spectra of all complexes one would expect a similar band pattern for **2a–c** resembling the solution spectra of high dr compounds **2b** and **2c**, whereas solid **2d** should deliver spectra of the Δ-(*S*) or Λ-(*R*) diastereomers. As suggested from the calculated spectra of pure diastereomers, the spectrum of solid **2d** should be different and look like the spectrum of calculated Λ-(*R*)-**2b** (Figure 7A,V), where the signals have an opposite sign compared to the corresponding diastereomer.

Solid-phase CD is generally challenging, because contributions from linear dichroism, linear birefringence, and scattering problems might adulterate the spectrum and make the interpretation difficult, requiring more sophisticated measurement protocols, or ideally, dedicated instrumentation for solid samples.[26] Nevertheless, interpretable solid-state ECD spectra can be obtained with commercial instruments,[27] provided that certain issues are taken into consideration: (i) scattering must be avoided. This was achieved by keeping the particle size as low as possible through vigorous grinding. In addition, the difference in refractive index between the sample and the surrounding matrix, in which the sample particles are dispersed, should be as small as possible. This is the case for KBr pellets, such as those traditionally used for infrared spectroscopy. (ii) Anisotropy effects from oriented crystals in the pellet may lead to linear birefringence artifacts. To minimize contributions from linear dichroism and linear birefringence, the sample pellet was placed in a home-built rotating sample holder. Spectra were recorded with very long detector integration time to level out angle-dependent birefringence contributions. Every pellet was measured on the front and reverse side, and averaged.

DOI: 10.1021/ic502661u
Inorg. Chem. 2015, 54, 2193–2203

The resulting solid-state CD spectra (Figure 7B,I–IV) are shown in comparison to the corresponding chloroform solution spectra in Figure 7A,I–IV. For **2a–c** the spectra look very similar and all bands have the same sign throughout the (*R*) and the (*S*) series, respectively. This not only indicates an identical absolute configuration at the copper ion in **2a–c** both in the solid and the solution state but also confirms the applicability of the solid-state CD protocol described above for these complexes. Solution and solid-state spectra of **2d** disagree significantly, indicating opposite metal-centered chirality (Figure 7A,IV and B,IV). As expected from the spectrum calculated for Λ-geometry (Figure 7A,V) the ligand–metal charge transfer bands at 270–415 nm have an opposite sign in the KBr pellet sample compared to chloroform solution. This is also confirmed by spectra obtained from TD-DFT calculations on the crystal structure geometries of Δ-(*R*)-**2b** and Λ-(*R*)-**2d** (Figure 7B,V), where a strong signal at ∼360 nm is positive for Δ-(*R*)-**2b** and negative for Λ-(*R*)-**2d**. Furthermore, the d–d transition signals between 500 and 700 nm have a different appearance for the solid and the solution state. In contrast to spectra of Δ-configured complexes such as Δ-(*R*)-**2b**, which exhibits a d–d transition maximum at 653 nm (Figure 7B,II), there is a strong negative contribution above 700 nm that blue-shifts the corresponding maximum to 620 nm (Figure 7B,IV). Therefore, the position of the CD maximum corresponding to the d–d transition correlates with the dr of the complexes: in solution spectra of (*R*)-**2a** and (*R*)-**2d** the maximum exhibits a more pronounced blue shift than in spectra of (*R*)-**2b** and (*R*)-**2c**. This indicates a larger amount of Λ-species present in solutions of (*R*)-**2a** and (*R*)-**2d** than in (*R*)-**2b** and (*R*)-**2c**, which exhibit a high dr in favor of Δ. Nevertheless, even though methoxy-substituted (*R*)-**2d** crystallizes with a Λ-configured copper ion, the results from VCD and CD spectroscopy indicate an excess of Δ-species in solution. This suggests that (*R*)-configured ligands in principle induce the Δ configuration at the copper ion (and (*S*)-configured ligands the Λ-configuration, respectively). The extent of induction is modulated by the choice of para substituent on the ligand leading to a shifted equilibrium of Δ- and Λ-configured conformers. In the solid state these inductive effects seem to be overridden by crystal lattice effects. As only one diastereomer for each complex crystallized and, hence, was available for solid-state structural analysis by single-crystal X-ray diffraction, we do not have a quantitative measure for such effects in this system. It is, however, evident that the packing in **2a–2d** is governed by weak supramolecular interactions that may result in subtle energetic differences between the two diastereomers. Only few $\pi-\pi$-stacking or C–H$\cdots\pi$ interactions are found between the molecules or pseudodimers (Supporting Information). Hence, we suggest that the homochirality of complexes **2** (i.e., the crystallization of only one diastereomer for each (*R*)- or (*S*)-ligand instead of Δ/Λ-cocrystallization) is due to the corrugated van der Waals surface of the molecules that allows for preferred interlocking of one molecular geometry over the other,[23d,28] which in turn determines metal-centered helicity. Therefore, considering that the energy differences between different conformers of salicylaldiminato complexes of copper(II) may be very small (Table 2), it is not surprising that a geometry with a minor population in solution is the one that crystallizes.

CONCLUSIONS

In this study, we used pseudotetrahedral chiral copper(II) complexes as a model for thermodynamically driven chirality transfer from chiral salicylaldimine ligands to metal-centered chirality. Using different chiroptical methods, namely, VCD and ECD spectroscopy, we could show that for salicylaldimine ligands with either no substituent, or a chlorine, bromine, or methoxy in para position of an aromatic ligand side-chain, a clear chiral induction was observed in solution for all four different variants, with an (*R*)-configured ligand leading to Δ-configured helicity, and an (*S*)-configured ligand leading to Λ-configured helicity. Taking into account the considerably small energy difference between different Δ and Λ-configured conformers from quantum chemical calculations (less than 3 kJ·mol^{-1} for the lowest-lying Δ- and Λ-conformers), we suggest that a conformational change gives rise to a configurational switch at the metal ion, provided that the resulting structure is energetically more favorable. Such a configurational switch can be triggered by a different environment. In this study, we present an example in which a conformation that is less populated in solution can be stabilized in a crystal lattice, thereby inducing the opposite metal-configuration as observed for very similar, but differently substituted salicylaldiminato ligands. These findings clearly demonstrate that in some cases it is not sufficient to determine the configuration of a compound by X-ray crystallography alone, because the solution structure can be different. This is of particular importance if compounds, such as chiral-at-metal complexes, are used as catalysts in stereoselective synthesis.

MATERIALS AND METHODS

Syntheses. *(R)- or (S)-N-(1-(4-X-phenyl)ethyl)salicylaldimines (**1a–d**).* Chiral ligands **1a–d** were obtained as yellow bright crystals as described previously.[10d,29] Analytical data (elementary analysis, ^{1}H NMR, IR) was in agreement with the literature data.

*Δ/Λ-Bis{(R)- or (S)-{N-(1-(4-X-phenyl)ethyl)salicylaldiminato-κ^{2}N,O}copper(II) (**2a–d**).* The addition of $Cu(NO_3)_2{\cdot}3H_2O$ (0.5 mmol) to a stirred solution of (*R*)- or (*S*)-*N*-(1-(4-X-phenyl)ethyl)-salicylaldimines (1 mmol) and triethylamine (140 μL, 1 mmol) in methanol (25 mL) produced a dark green solution. After the solution was stirred under reflux at 80 °C for 6 h, the resulting solution was allowed to cool to room temperature and filtered. The filtrate was evaporated slowly at room temperature. After 4 d, green crystals were isolated from the solution.

The crystalline complexes were tested for solubility in different solvents. Highly soluble in toluene, dimethylformamide (DMF), dioxin, CH_2Cl_2, tetrahydrofuran (THF), ethyl acetate, acetone, $CHCl_3$, MeOH, EtOH, CCl_4. Less soluble in cyclohexane, acetonitrile, diethyl ether, *n*-hexane, isopropanol. Not soluble in H_2O.

*(R)-Bis{N-(1-phenylethyl)salicylaldiminato-κ^{2}N,O}copper(II) ((R)-**2a**).* mp 145 °C. Yield: 0.42 g, 82%. $C_{30}H_{28}CuN_2O_2$ (512.8 g mol^{-1}): calculated C 70.36, H 5.51, N 5.47; found C 70.10, H 5.69, N 5.47%. IR (cm^{-1}): 3058.3 (vw), 3025.8 (vw), 2973.7 (vw), 2869.8 (vw), 2673.1 (vw), 2196.7 (vw), 2131.0 (vw), 1960.2 (vw), 1608.3 (vs), 1532.1 (m), 1493.8 (vw), 1444.1 (s), 1398.6 (w), 1321.9 (s), 1256.8 (vw), 1197.5 (m), 1137.0 (w), 1078.9 (w), 1023.0 (w), 977.8 (vw), 933.5 (w), 888.2 (w), 848.5 (w), 808.7 (vw), 748.9 (s), 695.3 (s), 592.2 (m), 517.1 (m), 455.6 (m).

*(S)-Bis{N-(1-phenylethyl)salicylaldiminato-κ^{2}N,O}copper(II) ((S)-**2a**).* mp 150 °C. Yield: 0.41 g, 80%. $C_{30}H_{28}CuN_2O_2$ (512.8 g mol^{-1}): calculated C 70.36, H 5.51, N 5.47; found C 70.02, H 5.71, N 5.45%. IR (cm^{-1}): 3058.3 (vw), 3025.8 (vw), 2973.7 (vw), 2869.8 (vw), 2673.1 (vw), 2196.7 (vw), 2131.0 (vw), 1960.2 (vw), 1608.3 (vs), 1532.1 (m), 1493.8 (vw), 1444.1 (s), 1398.6 (w), 1321.9 (s), 1256.8 (vw), 1197.5 (m), 1137.0 (w), 1078.9 (w), 1023.0 (w), 977.8

DOI: 10.1021/ic502661u
Inorg. Chem. 2015, 54, 2193–2203

(vw), 933.5 (w), 888.2 (w), 848.5 (w), 808.7 (vw), 748.9 (s), 695.3 (s), 592.2 (m), 517.1 (m), 455.6 (m)

*(R)-Bis{N-(1-(4-chlorophenyl)ethyl)salicylaldiminato-κ²N,O}-copper(II) ((R)-**2b**).* mp 158 °C. Yield: 0.47 g, 81%. $C_{30}H_{26}Cl_2CuN_2O_2$ (581.0 g mol^{-1}): calculated C 62.02, H 4.51, N 4.82; found C 61.80, H 4.64, N 4.76%. IR (cm^{-1}): 3733.8 (vw), 3008.8 (vw), 2971.3 (w), 2928.1 (vw), 2870.8 (vw), 2362.7 (w), 2336.4 (vw), 1935.5 (w), 1892.0 (w), 1616.2 (vs), 1596 3 (s), 1535.4 (m), 1488.1 (w), 1446.5 (s), 1392.9 (m), 1350.4 (w), 1328.2 (s), 1192.6 (m), 1147.1 (m), 1124.9 (m), 1081.8 (m), 1033.4 (w), 1010.1 (s), 968.3 (w), 923.0 (m), 886.1 (m), 818.5 (s), 779.7 (w), 732.7 (s), 656.4 (w), 623.8 (vw), 585.6 (m), 544.4 (s), 481.0 (m), 452.5 (m), 423.1 (m). $[\alpha]^{25}_{589}$ (c = 0.021 g/100 mL): −301.6°.

*(S)-Bis{N-(1-(4-chlorophenyl)ethyl)salicylaldiminato-κ²N,O}-copper(II) ((S)-**2b**).* mp 165 °C. Yield: 0.46 g, 79%. $C_{30}H_{26}Cl_2CuN_2O_2$ (581.0 g mol^{-1}): calculated C 62.02, H 4.51, N 4.82; found C 60.99, H 4.53, N 4.77%. IR (cm^{-1}): 3010.3 (vw), 2972.5 (w), 2361.6 (w), 2337.3 (w), 2105.1 (vw), 1891.8 (vw), 1618.1 (vs), 1598.2 (s), 1536.0 (s), 1489.8 (w), 1449.4 (s), 1395.5 (m), 1351.8 (m), 1331.4 (s), 1245.9 (vw), 1212.8 (w), 1193.0 (m), 1147.9 (m), 1126.1 (m), 1085.9 (m), 1031.2 (w), 1012.0 (m), 969.3 (m), 924.3 (m), 887.7 (m), 849.4 (w), 820.6 (s), 780.2 (m), 748.3 (s), 735.2 (s), 719.7 (m), 656.9 (m), 624.6 (w), 588.1 (m), 546.5 (s), 482.5 (m), 453.8 (m), 424.8 (m) . $[\alpha]^{25}_{589}$ (c = 0.020 g/100 mL): +296.0°.

*(R)-Bis{N-(1-(4-bromophenyl)ethyl)salicylaldiminato-κ²N,O}-copper(II) ((R)-**2c**).* mp 192 °C. Yield: 0.52 g, 78%. $C_{30}H_{26}Br_2CuN_2O_2$ (669.9 g mol^{-1}): calculated C 53.79, H 3.91, N 4.18; found C 53.50, H 3.96, N 4.11%. IR (cm^{-1}): 2971.7 (w), 1618.3 (vs), 1597.8 (s), 1535.4 (s), 1487.8 (m), 1449.6 (s), 1395.0 (m), 1352.3 (m), 1330.9 (s), 1246.3 (w), 1193.9 (m), 1147.7 (m), 1126.0 (m), 1072.5 (m), 1030.9 (w), 1008.6 (s), 968.7 (w), 924.0 (m), 887.2 (m), 849.3 (w), 817.8 (s), 775.0 (w), 749.0 (s), 734.9 (s), 717.1 (m), 587.9 (s), 540.1 (s), 473.4 (w), 451.2 (w). $[\alpha]^{25}_{589}$ (c = 0.018 g/100 mL): −241.8°.

*(S)-Bis{N-(1-(4-bromophenyl)ethyl)salicylaldiminato-κ²N,O}-copper(II) ((S)-**2c**).* mp 195 °C. Yield: 0.53 g, 79%. IR (cm^{-1}): 3025.0 (w), 2971.6 (w), 1622.7 (vs), 1601.1 (vs), 1537.5 (vs), 1489.1 (m), 1466.5 (s), 1452.3 (vs), 1398.0 (m), 1353.5 (s), 1335.1 (vs), 1247.2 (w), 1194.7 (m), 1149.2 (s), 1128.2 (m), 1075.5 (s), 1030.7 (w), 1010.5 (s), 971.1 (w), 926.1 (m), 889.0 (w), 822.4 (s), 774.4 (w), 751.8 (s), 736.6 (m), 718.6 (w), 590.5 (m), 542.6 (m), 453.3 (w). $[\alpha]^{25}_{589}$ (c = 0.014 g/100 mL): +242.6°.

*(R)-Bis{N-(1-(4-methoxyphenyl)ethyl)salicylaldiminato-κ²N,O}-copper(II) ((R)-**2d**).* mp 145 °C. Yield: 0.47 g, 82%. $C_{32}H_{32}CuN_2O_2$ (572.2 g mol^{-1}): calculated C 67.18, H 5.64, N 4.90; found C 66.61, H 5.73, N 4.87%. IR (cm^{-1}): 3013.8 (vw), 2937.2 (vw), 2890.9 (vw), 2836.3 (w), 1609.5 (vs), 1536.3 (m), 1511.6 (s), 1466.5 (m), 1444.3 (s), 1396.2 (w), 1340.5 (m), 1318.0 (w), 1297.0 (m), 1246.3 (s),1194.0 (m), 1179.8 (m), 1145.9 (s), 1125.4 (m), 1067.0 (w), 1020.6 (m), 936.8 (w), 885.8 (m), 840.0 (m), 755.2 (vs), 589.6 (m), 551.9 (m), 511.9 (m), 455.9 (m), 423.3 (w). $[\alpha]^{25}_{589}$ (c = 0.019 g/100 mL): +187.0°.

*(S)-Bis{N-(1-(4-methoxyphenyl)ethyl)salicylaldiminato-κ²N,O}-copper(II) ((S)-**2d**).* mp 182 °C. Yield: 0.46 g, 80%. $C_{32}H_{32}CuN_2O_2$ (572.2 g mol^{-1}): calculated C 67.18, H 5.64, N 4.90; found C 66.55, H 5.81, N 4.82%. IR (cm^{-1}): 3015.0 (vw), 2939.6 (vw), 2895.3 (vw), 2835.6 (w), 1606.9 (vs), 1510.0 (m), 1442.6 (s), 1395.5 (w), 1309.4 (w), 1243.4 (s), 1186.7 (m), 1140.7 (m), 1066.1 (w), 1019.2 (m), 931.0 (w), 885.0 (m), 838.7 (m), 750.5 (vs), 586.5 (m), 546.9 (m), 510.8 (m), 455.6 (m), 421.4 (w). $[\alpha]^{25}_{589}$ (c = 0.019 g/100 mL): −186.6°.

X-ray Crystallography. Crystals of the complexes suitable for X-ray diffractometry were carefully selected under a polarizing microscope and picked with the tip of a needle. Single-crystal data were collected at 203(2) K on a Bruker AXS equipped with a APEXII CCD area-detector with Mo Kα radiation (λ = 0.710 73 Å). The empirical absorption corrections were applied using the SADABS program.[30] The structures were solved using the direct method (SHELXS-97),[31] which located the positions of all non-hydrogen atoms. These were refined anisotropically. All the hydrogen atoms of the ligands were placed in calculated positions with fixed isotropic thermal parameters and included in structure factor calculations in the final stage of a full-matrix least-squares refinement. The detailed crystallographic data including the Flack parameter indicating reliability of the absolute configuration[8] are listed in the Supporting Information.

Quantum Chemical Calculations. For calculation of a potential energy surface (PES) of Δ-conformers the crystal structure Δ-(*R*)-bis{*N*-(1-(4-chlorophenyl)ethyl)salicylaldiminato-κ²*N*,*O*}copper(II) (Δ-(*R*)-**2b**) was used as a template. We calculated a single point energy for the starting geometries and the energy and angle θ after 20 optimization steps for all rotational angles φ1 and φ2 around the two N−Cα bonds (Figure 2) in increments of 20° at the B3LYP-level, using the Ahlrichs VTZ[24] basis set for copper and 6-31G(d) for all other atoms in GAUSSIAN 09.[25] For the PES of Λ-(*R*)-**2b**, we used a model based on the mirror image of the crystal structure of Δ-(*R*)-**2b** and inverted stereocenters at both Cα. The PES and θ 2D maps were generated using the default triangulation/linear interpolation algorithm in Origin 9 (OriginLab Corporation, Northampton, MA, USA). For full geometry optimization at the B3LYP/Ahlrichs VTZ, 6-31G(d) level we picked a representative geometry from each region on the 2D map where partially optimized structures were clustered together around a putative relative minimum. After full optimization the unique geometries that accounted for more than 1% population calculated from their Boltzmann weights (4 Δ-conformers, 2 Λ-conformers) were picked for a second optimization and calculation of IR and VCD spectra at the B3LYP/Ahlrichs VTZ, 6-31+G(d,p) level. The calculated frequencies were scaled by 0.97 for vibrational spectra and calculation of thermochemical parameters. For calculation of relative free energies (ΔG) the thermochemical parameters were corrected for contributions from internal rotations. Theoretical IR and VCD spectra were constructed by using a Lorentzian bandwidth of 6 cm^{-1} around the calculated intensities. Excited-state ECD calculations at the TD-DFT level (B3LYP/Ahlrichs VTZ, 6-31+G(d,p)) were performed in Gaussian 09 on the optimized geometries of (*R*)-**2b**, found by the procedure described above, and on the crystal structure geometries of Δ-(*R*)-**2b** and Λ-(*R*)-**2d**. For each geometry 60 excited states were taken into consideration. The spectra were constructed with Gaussian line shape and an exponential half-width of 0.16 eV in SpecDis.[32] For better comparison to experimental spectra, the calculated spectra were λ-shifted by 10 nm. For Boltzmann-averaging of ECD spectra the same weights were used as for VCD.

IR and VCD Measurements. IR spectra of KBr pellets of (*R*)- and (*S*)-**2a**−**d** were measured on a Bruker IFS25 FTIR spectrometer. IR and VCD 4 cm^{-1} resolution spectra of $CDCl_3$ solutions of (*R*)-**2a** (38 mM), (*R*)-**2b** and (*S*)-**2b** (44 mM), and (*R*)-**2c** (37 mM) were measured in a 100 μm BaF_2 cell on a ChiraIR Dual-PEM VCD spectrometer from BioTools (data collection time: 4 h). The spectra of (*S*)-**2a** (32 mM), (*S*)-**2c** (37 mM), and (*R*)-**2d** (40 mM) were recorded on a Bruker Tensor 27 FTIR spectrometer equipped with the Bruker PMA 50 VCD side bench module (data collection time: 10 h). All spectra were corrected for background effects by solvent subtraction. The optimum retardation value of the photoelastic modulator (PEM) was set at 1400 cm^{-1}, which is near the middle of the observed spectral range (1800−800 cm^{-1}).

Ultraviolet−Visible and Circular Dichroism Measurements. UV−vis and CD spectra of $CHCl_3$ solutions of the free salicylaldimine ligands **1a**−**d** (c = 5 × 10^{-4} mol L^{-1}) and the corresponding copper(II) complexes (c = 1.5 × 10^{-4} mol L^{-1} (**2a**); 1.3 × 10^{-4} mol L^{-1} (**2b**); 1.0 × 10^{-4} mol L^{-1} (**2c**); 2.5 × 10^{-4} mol L^{-1} (**2d**)) were recorded in a 1 cm path length quartz cell (Hellma, Müllheim, Germany) on a JASCO J-810 spectropolarimeter in the spectral range from 200 to 800 nm and were averaged over three accumulations. Solid-state CD measurements of **2a**−**d** were performed with KBr pellets (0.1% w/w) in the spectral range from 220 to 800 nm. During a measurement the pellet was rotated (20 rpm) using a motor-driven sample cell holder at a detector integration time of 16 s (scan rate: 20 nm min^{-1}). Contributions from linear dichroism and linear birefringence that are independent from the rotation angle[26b] were evaluated by measuring both sides of the pellet. Because the difference between the front- and reverse-side measurements was negligible in all

DOI: 10.1021/ic502661u
Inorg. Chem. 2015, 54, 2193−2203

samples, the angle-independent contributions were considered to be small, and the front- and reverse-side spectra were averaged.

■ ASSOCIATED CONTENT

Supporting Information

Details of X-ray crystal data and refinement with atom-labeled molecular structure figures, crystal packing analysis, optimized DFT geometries. This material is available free of charge via the Internet at http://pubs.acs.org.

■ AUTHOR INFORMATION

Corresponding Author

*E-mail: steffen.luedeke@pharmazie.uni-freiburg.de. Phone: +49 (0)761 203-67398. Fax: +49 (0)761 203-6351.

Author Contributions

The manuscript was written through contributions of all authors. All authors have given approval to the final version of the manuscript.

Notes

The authors declare no competing financial interest.

■ ACKNOWLEDGMENTS

We acknowledge the use of the computing resources provided by the Black Forest Grid Initiative.

■ REFERENCES

(1) Campos, K. R.; Lee, S.; Journet, M.; Kowal, J. J.; Cai, D. W.; Larsen, R. D.; Reider, P. J. *Tetrahedron Lett.* **2002**, *43*, 6957−6959.

(2) Korevaar, P. A.; George, S. J.; Markvoort, A. J.; Smulders, M. M. J.; Hilbers, P. A. J.; Schenning, A. P. H. J.; De Greef, T. F. A.; Meijer, E. W. *Nature* **2012**, *481*, 492−496.

(3) Akine, S.; Hotate, S.; Nabeshima, T. *J. Am. Chem. Soc.* **2011**, *133*, 13868−13871.

(4) (a) Knof, U.; von Zelewsky, A. *Angew. Chem., Int. Ed.* **1999**, *38*, 302−322. (b) Mamula, O.; von Zelewsky, A.; Bark, T.; Stoeckli-Evans, H.; Neels, A.; Bernardinelli, G. *Chem.—Eur. J.* **2000**, *6*, 3575−3585.

(5) (a) Ernst, R. E.; O'Connor, M. J.; Holm, R. H. *J. Am. Chem. Soc.* **1967**, *89*, 6104−6113. (b) Sakiyama, H.; Okawa, H.; Matsumoto, N.; Kida, S. *Dalton Trans.* **1990**, 2935−2939. (c) Sakiyama, H.; Okawa, H.; Matsumoto, N.; Kida, S. *Bull. Chem. Soc. Jpn.* **1991**, *64*, 2644−2647.

(6) (a) Constable, E. C.; Housecroft, C. E.; Kulke, T.; Lazzarini, C.; Schofield, E. R.; Zimmermann, Y. *Dalton Trans.* **2001**, 2864−2871. (b) Constable, E. C.; Housecroft, C. E.; Jullien, V.; Neuburger, M.; Poleschak, I.; Reymann, S.; Saxer, S.; Schaffner, S. *Polyhedron* **2007**, *26*, 5519−5526. (c) Chow, H. S.; Constable, E. C.; Frantz, R.; Housecroft, C. E.; Lacour, J.; Neuburger, M.; Rappoport, D.; Schaffner, S. *New J. Chem.* **2009**, *33*, 376−385. (d) Constable, E. C.; Zhang, G. Q.; Housecroft, C. E.; Neuburger, M.; Zampese, J. A. *Chem. Commun.* **2010**, *46*, 3077−3079. (e) Constable, E. C. *Chem. Soc. Rev.* **2013**, *42*, 1637−1651. (f) Brewer, G.; Brewer, C.; Butcher, R. J.; Robichaux, G. T.; Viragh, C. *Inorg. Chim. Acta* **2014**, *410*, 171−177.

(7) Cross, R. J.; Farrugia, L. J.; Newman, P. D.; Peacock, R. D.; Stirling, D. *Dalton Trans.* **1996**, 4449.

(8) (a) Flack, H. D. *Acta Crystallogr., Sect. A* **1983**, *39*, 876−881. (b) Flack, H. D.; Bernardinelli, G. *Acta Crystallogr., Sect. A* **1999**, *55*, 908−915. (c) Flack, H. D.; Bernardinelli, G. *Chirality* **2008**, *20*, 681−690. (d) Flack, H. D.; Sadki, M.; Thompson, A. L.; Watkin, D. J. *Acta Crystallogr., Sect. A* **2011**, *67*, 21−34.

(9) (a) Kaizaki, S., Applications of Electronic Circular Dichroism to Inorganic Stereochemistry. In *Comprehensive Chiroptical Spectroscopy;* Berova, N.; Polavarapu, P. L.; Nakanishi, K.; Woody, R. W., Eds.; John Wiley & Sons, Inc.: Hoboken, NJ, 2012; Vol. 2, pp 451−471. (b) Enamullah, M.; Uddin, A. K. M. R.; Pescitelli, G.; Berardozzi, R.; Makhloufi, G.; Vasylyeva, V.; Chamayou, A. C.; Janiak, C. *Dalton Trans.* **2014**, *43*, 3313−3329.

(10) (a) Lassen, P. R.; Guy, L.; Karame, I.; Roisnel, T.; Vanthuyne, N.; Roussel, C.; Cao, X. L.; Lombardi, R.; Crassous, J.; Freedman, T. B.; Nafie, L. A. *Inorg. Chem.* **2006**, *45*, 10230−10239. (b) Stephens, P. J.; Devlin, F. J.; Villani, C.; Gasparrini, F.; Mortera, S. L. *Inorg. Chim. Acta* **2008**, *361*, 987−999. (c) Sato, H.; Mori, Y.; Fukuda, Y.; Yamagishi, A. *Inorg. Chem.* **2009**, *48*, 4354−4361. (d) Chamayou, A. C.; Lüdeke, S.; Brecht, V.; Freedman, T. B.; Nafie, L. A.; Janiak, C. *Inorg. Chem.* **2011**, *50*, 11363−11374. (e) Wu, T.; Zhang, X. P.; Li, C. H.; Bouř, P.; Li, Y. Z.; You, X. Z. *Chirality* **2012**, *24*, 451−458. (f) Merten, C.; Xu, Y. J. *Dalton Trans.* **2013**, *42*, 10572−10578. (g) Merten, C.; McDonald, R.; Xu, Y. *Inorg. Chem.* **2014**, *53*, 3177−3182.

(11) (a) Werner, A. *Ber. Dtsch. Chem. Ges.* **1911**, *44*, 1887. (b) Werner, A. *Ber. Dtsch. Chem. Ges.* **1914**, *47*, 3087.

(12) Berova, N.; Di Bari, L.; Pescitelli, G. *Chem. Soc. Rev.* **2007**, *36*, 914−931.

(13) (a) Okawa, H.; Nakamura, M.; Kida, S. *Inorg. Chim. Acta* **1986**, *120*, 185−189. (b) Akitsu, T.; Einaga, Y. *Polyhedron* **2005**, *24*, 2933−2943. (c) Dragna, J. M.; Pescitelli, G.; Tran, L.; Lynch, V. M.; Anslyn, E. V.; Di Bari, L. *J. Am. Chem. Soc.* **2012**, *134*, 4398−4407.

(14) Sato, H.; Taniguchi, T.; Nakahashi, A.; Monde, K.; Yamagishi, A. *Inorg. Chem.* **2007**, *46*, 6755−6766.

(15) (a) Bauer, E. B. *Chem. Soc. Rev.* **2012**, *41*, 3153−3167. (b) Chen, L. A.; Xu, W. C.; Huang, B.; Ma, J. J.; Wang, L.; Xi, J. W.; Harms, K.; Gong, L.; Meggers, E. *J. Am. Chem. Soc.* **2013**, *135*, 10598−10601.

(16) Feng, L.; Geisselbrecht, Y.; Blanck, S.; Wilbuer, A.; Atilla-Gokcumen, G. E.; Filippakopoulos, P.; Kräling, K.; Celik, M. A.; Harms, K.; Maksimoska, J.; Marmorstein, R.; Frenking, G.; Knapp, S.; Essen, L. O.; Meggers, E. *J. Am. Chem. Soc.* **2011**, *133*, 5976−5986.

(17) Albrecht, M.; Isaak, E.; Baumert, M.; Gossen, V.; Raabe, G.; Fröhlich, R. *Angew. Chem., Int. Ed.* **2011**, *50*, 2850−2853.

(18) Álvarez, C. M.; Carrillo, R.; García-Rodríguez, R.; Miguel, D. *Chem. Commun.* **2011**, *47*, 12765−12767.

(19) Zahn, S.; Canary, J. W. *Science* **2000**, *288*, 1404−1407.

(20) Downing, R. S.; Urbach, F. L. *J. Am. Chem. Soc.* **1969**, *91*, 5977−5983.

(21) (a) Vigato, P. A.; Tamburini, S. *Coord. Chem. Rev.* **2004**, *248*, 1717−2128. (b) Gupta, K. C.; Sutar, A. K.; Lin, C.-C. *Coord. Chem. Rev.* **2009**, *253*, 1926−1946. (c) Hou, X. K.; Wu, L. F.; Xiao, H. P.; Li, M. X.; Zhu, S. R.; Wang, Z. X. *Z. Anorg. Allg. Chem.* **2013**, *639*, 633−636. (d) Matsunaga, S.; Shibasaki, M. *Chem. Commun.* **2014**, *50*, 1044−1057. (e) Moriwaki, H.; Resch, D.; Li, H. G.; Ojima, I.; Takeda, R.; Aceña, J. L.; Soloshonok, V. A. *Beilstein J. Org. Chem.* **2014**, *10*, 442−448.

(22) Enamullah, M.; Vasylyeva, V.; Janiak, C. *Inorg. Chim. Acta* **2013**, *408*, 109−119.

(23) (a) Hosseini Monfared, H.; Vahedpour, M.; Yeganeh, M. M.; Ghorbanloo, M.; Mayer, P.; Janiak, C. *Dalton Trans.* **2011**, *40*, 1286−1294. (b) Hosseini Monfared, H.; Kalantari, Z.; Kamyabi, M. A.; Janiak, C. *Z. Anorg. Allg. Chem.* **2007**, *633*, 1945−1948. (c) Masui, H. *Coord. Chem. Rev.* **2001**, *219*, 957−992. (d) Janiak, C.; Chamayou, A. C.; Uddin, A. K. M. R.; Uddin, M.; Hagen, K. S.; Enamullah, M. *Dalton Trans.* **2009**, 3698−3709.

(24) Schäfer, A.; Horn, H.; Ahlrichs, R. *J. Chem. Phys.* **1992**, *97*, 2571−2577.

(25) Frisch, M. J.; Trucks, G. W.; Schlegel, H. B.; Scuseria, G. E.; Robb, M. A.; Cheeseman, J. R.; Scalmani, G.; Barone, V.; Mennucci, B.; Petersson, G. A.; Nakatsuji, H.; Caricato, M.; Li, X.; Hratchian, H. P.; Izmaylov, A. F.; Bloino, J.; Zheng, G.; Sonnenberg, J. L.; Hada, M.; Ehara, M.; Toyota, K.; Fukuda, R.; Hasegawa, J.; Ishida, M.; Nakajima, T.; Honda, Y.; Kitao, O.; Nakai, H.; Vreven, T.; Montgomery, J. A., Jr.; Peralta, J. E.; Ogliaro, F.; Bearpark, M.; Heyd, J. J.; Brothers, E.; Kudin, K. N.; Staroverov, V. N.; Kobayashi, R.; Normand, J.; Raghavachari, K.; Rendell, A.; Burant, J. C.; Iyengar, S. S.; Tomasi, J.; Cossi, M.; Rega, N.; Millam, N. J.; Klene, M.; Knox, J. E.; Cross, J. B.; Bakken, V.; Adamo, C.; Jaramillo, J.; Gomperts, R.; Stratmann, R. E.; Yazyev, O.; Austin, A. J.; Cammi, R.; Pomelli, C.; Ochterski, J. W.; Martin, R. L.; Morokuma, K.; Zakrzewski, V. G.; Voth, G. A.; Salvador, P.;

DOI: 10.1021/ic502661u
Inorg. Chem. 2015, 54, 2193−2203

Dannenberg, J. J.; Dapprich, S.; Daniels, A. D.; Farkas, Ö.; Foresman, J. B.; Ortiz, J. V.; Cioslowski, J.; Fox, D. J. *GAUSSIAN 09,* Revision B.01; Gaussian, Inc.: Wallingford, CT, 2009.
(26) (a) Kuroda, R.; Honma, T. *Chirality* **2000**, *12*, 269−277. (b) Kuroda, R.; Harada, T., Solid-State Chiroptical Spectroscopy: Principles and Applications. In *Comprehensive Chiroptical Spectroscopy;* Berova, N.; Polavarapu, P. L., Nakanishi, K., Woody, R. W., Eds. John Wiley & Sons, Inc.: Hoboken, NJ, 2012; Vol. *1*, pp 91−113.
(27) (a) Pescitelli, G.; Kurtan, T.; Florke, U.; Krohn, K. *Chirality* **2009**, *21*, E181−E201. (b) Hussain, H.; Ahmed, I.; Schulz, B.; Draeger, S.; Florke, U.; Pescitelli, G.; Krohn, K. *Chirality* **2011**, *23*, 617−623.
(28) Enamullah, M.; Sharmin, A.; Hasegawa, M.; Hoshi, T.; Chamayou, A. C.; Janiak, C. *Eur. J. Inorg. Chem.* **2006**, 2146−2154.
(29) Enamullah, M.; Uddin, A. K. M. R.; Chamayou, A. C.; Janiak, C. *Z. Naturforsch., B: Chem. Sci.* **2007**, *62*, 807−817.
(30) Sheldrick, G. M. *SADABS;* University of Göttingen: Göttingen, Germany, 1996.
(31) Sheldrick, G. M. *Acta Crystallogr., Sect. A* **2008**, *64*, 112−122.
(32) Bruhn, T.; Schaumlöffel, A.; Hemberger, Y.; Bringmann, G. *Chirality* **2013**, *25*, 243−249.

DOI: 10.1021/ic502661u
Inorg. Chem. 2015, 54, 2193−2203